



Cite this: *Phys. Chem. Chem. Phys.*,
2016, 18, 10792

Elucidation of adsorption processes at the surface of Pt(331) model electrocatalysts in acidic aqueous media[†]

Marcus D. Pohl,^a Viktor Colic,^a Daniel Scieszka^{ab} and Aliaksandr S. Bandarenka^{*ab}

The Pt(331) surface has long been known to be the most active pure metal electrocatalyst for the oxygen reduction reaction (ORR) in acidic media. Its activity is often higher than those known for the Pt-based alloys towards ORR, being comparable with the most active Pt₃Ni(111), Pt₃Y or Pt₅Gd, and being more active than e.g. polycrystalline Pt₃Ni. Multiple active sites at this surface offer adsorption energies which are close to the optimal binding energy with respect to the main ORR intermediates; nevertheless, the exact location of these sites is still not clear. Taking into account the unique surface geometry of Pt(331), some adsorbates (including some oxygenated ORR-intermediates) should also contribute to the electronic structure of the neighbouring catalytic centres. However, the experimental elucidation of the specific adsorption of oxygenated species at this surface appears to be a non-trivial task. Such information holds the keys to the understanding of the high activity of this material and would enable the rational design of nanostructured ORR catalysts even without alloying. In this work, the electrified Pt(331)/electrolyte interface has been characterised using cyclic voltammetry (CV) combined with potentiodynamic electrochemical impedance spectroscopy (PDEIS) in 0.1 M HClO₄ solutions. The systems were studied in the potential region between 0.05 V and 1.0 V vs. RHE, where the adsorption of *H, *OH and *O species is possible in both O₂-free and O₂-saturated electrolytes. Our CV and PDEIS results support the hypothesis that in contrast to Pt(111), many Pt(331) surface sites are likely blocked by *O species at the polymer electrolyte membrane fuel cell benchmark potential of 0.9 V (RHE). We propose a model illustrated by simplified adsorbate structures at different electrode potentials, which is, however, able to explain the voltammetric and impedance data, and which is in good agreement with previously reported electrocatalytic measurements.

Received 27th December 2015,
Accepted 12th February 2016

DOI: 10.1039/c5cp08000b

www.rsc.org/pccp

Introduction

The oxygen reduction reaction (ORR) is one of the fundamental reactions for the realization of a sustainable provision of renewable energy.^{1–13} It is, for instance, of extreme importance for the so-called polymer electrolyte membrane fuel cells (PEMFCs),^{2,6,14–16} where it takes place at the cathode^{2,4,17–19} and largely limits the fuel cells' performance.^{2,17–20} This is mainly because of the relatively slow kinetics of the ORR, even if state-of-the-art platinum cathode electrocatalysts are used.^{6,8,17–19,21–24} The ORR in PEMFCs normally proceeds through at least three adsorbed intermediates, *OOH, *O, and *OH, towards molecular water (* denotes the adsorbed species).^{4,14,20,23,25}

The latter species are localized at specific catalytic centers on the surface. The nature, structure, electronic properties and relative surface abundance of these sites determine the observed activity, selectivity and stability of the catalytic materials.^{1,20} If these specific centers are identified, recent methodological advances and synthetic innovations would likely enable a relatively easy optimization of electro-catalysts.^{4,9,20,26,27} Alternatively, one would be able to create nanostructured materials with a maximal density of these centers at the surface.^{28–31} Therefore, single crystal surfaces, which offer a methodologically easier approach for the identification of active sites, are indispensable model objects on the way to a better understanding and optimization of nanostructured electrocatalysts.

Platinum is one of only a few materials known to offer a good balance between high ORR activity, required selectivity, and stability in aggressive acidic media necessary for modern PEMFCs.^{1,4,25,32,33} According to state-of-the-art models, the high activity of Pt is possibly due to the fact that the adsorption energies of the main intermediates (mentioned above) at the

^a Physik-Department ECS, Technische Universität München, James-Franck-Straße 1, 85748 Garching, Germany. E-mail: bandarenka@ph.tum.de

^b Nanosystems Initiative Munich (NIM), Schellingstraße 4, 80799 Munich, Germany

† Electronic supplementary information (ESI) available: Further experimental details and supporting experimental data. See DOI: 10.1039/c5cp08000b



surface are quite close to the optimum.^{34,35} These models also suggest that the most active sites are located at the Pt(111) facets, which bind *e.g.* *OH just ~ 0.1 eV stronger than the optimal binding energy.^{4,20,36} The active sites themselves can be roughly localized and described as “on-top” adsorption sites at the Pt(111) surface.^{37–41} These models recently facilitated the discovery of a series of promising Pt-alloys and nanostructured materials to catalyze the ORR.^{27,36,42–46} However, there are some highly active materials which seemingly contradict the above-mentioned theories.^{7,47,48}

Remarkably, the most active surface towards the ORR known to date is Pt(331), which can also be designated as Pt[3(111) \times (111)], and belongs to the family of these “unusual” catalysts.^{20,48} The ORR activity of Pt(331) is ~ 4.5 times better than that of Pt(111) at the PEMFC-benchmark electrode potential of 0.9 V (RHE), being more active than multiple Pt-alloy electrocatalysts.⁴⁸ While fcc(331) is known to be a surface with an extremely high density of steps, it seems logical that the defects themselves and not the (111)-terraces are the most active sites, similar to some other electrocatalytic reactions.^{49–52} This contradicts the finding that a surface with an even higher density of steps, Pt(110), shows an ORR activity similar to that measured for Pt(111).^{7,20,47,48}

The origin of these surprising experimental facts is still under debate. Several theoretical models have been elaborated based on explicit density functional theory (DFT) calculations (see *e.g.* ref. 53). Recently, it has been suggested that steps at platinum surfaces should likely be blocked by oxygenated species at “very early” electrode potentials.^{20,54} Most probably the blockage should occur after the desorption of underpotentially deposited hydrogen species in the range between ~ 0.05 V and ~ 0.4 V (RHE) in O₂-free acidic electrolytes,^{4,20,54} although these assumptions remain somewhat controversial. Based on the former hypothesis and experimental data, it has been demonstrated that the observed trends in the activities of Pt[n(111) \times (111)] and Pt[n(111) \times (100)] can be explained within the existing theoretical framework.²⁰ This is further supported by the hypothesis that the active sites are located at the (111) terraces.^{20,55} The (111) terraces of Pt(331) indeed provide almost optimal binding energy with respect to the ORR intermediates.²⁰ However, it is not clear why the electronic structure at these terraces is so different compared to Pt(111). One of the possible explanations is that some adsorbates (even some oxygenated ORR-intermediates) likely contribute to the electronic structure of the neighbouring catalytic centres.

Nevertheless, the exact adsorbate structures developed at different electrode potentials relevant for PEMFC applications at Pt(331) surfaces are still not known. The main difficulty is that it has been so far impossible to visualize these structures *in situ*, in liquid electrolytes or at elevated temperatures using *e.g.* electrochemical scanning tunneling microscopy. One of the main reasons is that the intermediate species (for instance *OH) are mobile and are basically a part of the first H₂O layer on the electrode.^{56–61} However, using other experimental techniques and some reference points, provided by numerous quantum chemistry calculations available in the literature, it

might still be possible to develop a better understanding of these structures and their role in ORR electrocatalysis.

In this work we propose a model employing simplified adsorbate structures at different electrode potentials at the Pt(331) surface based on voltammetric and potentiodynamic electrochemical impedance spectroscopy data obtained in O₂-free and O₂-saturated HClO₄ electrolytes. This model is capable of explaining the experimental results, and is in good agreement with previously reported electrocatalytic measurements.

Experimental

A bead-type Pt(331) crystal (icryst, Jülich, Germany) and a Pt(111) single crystal (5 mm in diameter, Mateck, Jülich, Germany) were used for all experiments. The crystals were flame-annealed using a butane–propane flame and cooled down in a mixture of 1000 ppm CO (4.7, Air Liquide, Germany) and Ar (5.0, Air Liquide, Germany). The status of the surface was assessed by characteristic voltammograms obtained in Ar-saturated HClO₄ electrolytes.

The electrochemical cell used in this work is described in detail in the ESI.† Before the experiments, all glassware was cleaned with a 3 : 1 mixture of H₂SO₄ and H₂O₂ (both Suprapur, Merck, Germany) and subsequently rinsed multiple times with ultrapure water obtained from an Evoqua Ultra Clear 10 TWF 30 UV (Evoqua, Germany) water purification system. A VSP-300 potentiostat (Bio-Logic, France) was used to control all electrochemical measurements.

The working electrodes were introduced into the electrolytes under potential control at 0.05 V *vs.* RHE. Cyclic voltammetry (CV) was performed at a scan rate of 50 mV s^{−1} in Ar-saturated solutions (Ar 5.0, Air Liquide, Germany).

A mercury–mercurous sulfate electrode (MMS) (SI Analytics, Germany) was used as a reference electrode. It was kept in a separate compartment filled with 0.1 M HClO₄ and separated from the working electrolyte by an ionically conducting ceramic insert. A polycrystalline Pt-wire was used as a counter electrode. All potentials in this paper are referenced to the RHE scale.

0.1 M HClO₄ aqueous solutions were used as working electrolytes. They were prepared from 70% HClO₄ (Suprapur, Merck, Germany), respectively, by diluting them with ultrapure water.

EIS measurements were performed in O₂-free and O₂-saturated (O₂ 5.0, Air Liquide, Germany) 0.1 M HClO₄ electrolytes in the frequency range between 30 kHz and 10 Hz and a 10 mV amplitude of the probing signals. Issues related to modeling and fitting of large experimental EIS datasets are reported in detail elsewhere⁶² and also presented in the ESI.† The quality of the measured impedance spectra was evaluated using the “linear”⁶³ and “logarithmic”⁶⁴ Kramers–Kronig check procedures.

The output of the fitting procedure was controlled by the root-mean-square deviations and estimated individual parameter errors using the “EIS Data Analysis 1.0” software, in order to ensure the validity of the model and the correctness of the fitting, as described in detail elsewhere.^{65,66}



Results

Cyclic voltammetry experiments

Fig. 1A shows the typical cyclic voltammograms of Pt(111) and Pt(331) in 0.1 M HClO₄. For both electrodes one can distinguish two regions where pairs of reversible peaks appear. For the Pt(111) electrode, the well-known symmetrical peaks due to hydrogen adsorption and desorption at more negative potentials between ~0.05 V and ~0.4 V are visible. However, Pt(331) reveals different distribution of adsorption energies in that range. At more positive potentials OH-adsorption on Pt(111) manifests itself as a pair of the so-called “butterfly” peaks between ~0.55 V and ~0.9 V with sharp features at ~0.8 V.⁶⁷ In contrast, the Pt(331) CVs are featureless in that region, with wide but relatively small peaks.

Integration of the respective anodic voltammetric currents (with the correction for the double layer capacitive current) reveals a difference in the charge of ~30 $\mu\text{C cm}^{-2}$. Pt(331) gives a charge of ~190 $\mu\text{C cm}^{-2}$ while Pt(111) gives a charge of only ~160 $\mu\text{C cm}^{-2}$ at the potentials of the anodic processes completed at the more negative potential region (Fig. 1B).

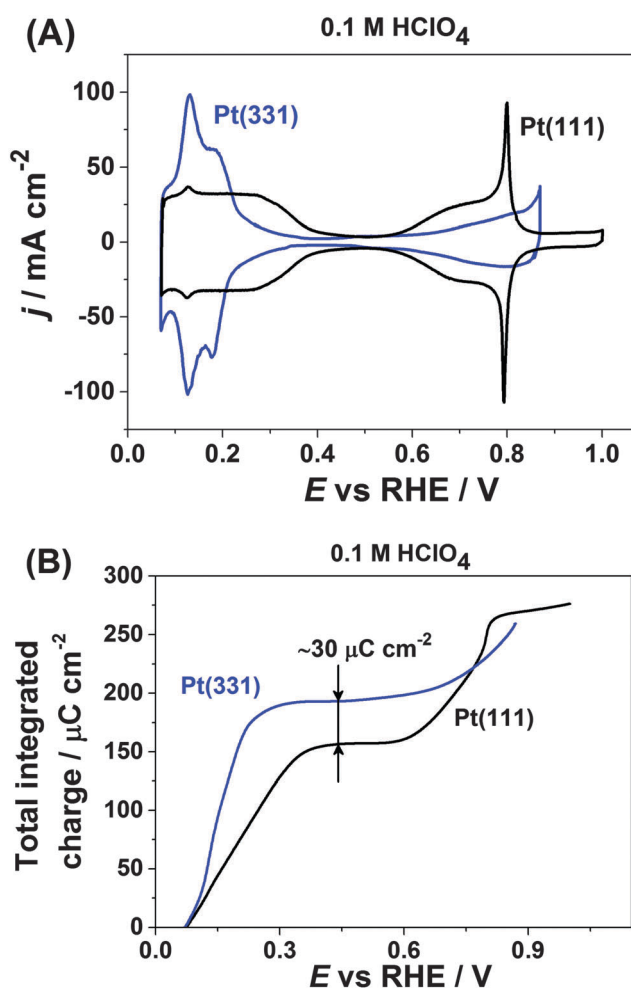


Fig. 1 (A) Typical cyclic voltammograms of Pt(111) and Pt(331) in 0.1 M HClO₄ and (B) integrated anodic parts of the corresponding voltammograms (corrected for the double layer capacitive current, $dE/dt = 50 \text{ mV s}^{-1}$).

However, at the key electrode potential of ~0.9 V for PEMFC applications the net anodic charges obtained from the integration of both CVs appeared to be approximately similar, ~280 $\mu\text{C cm}^{-2}$.

Potentiodynamic impedance spectroscopy experiments

In order to shed further light on the origin of the difference in the adsorption behavior between Pt(111) and Pt(331) electrodes, PDEIS experiments⁶⁸ were performed using Pt(331) surfaces. It is well known that impedance measurements cannot distinguish the double layer capacitance charging and the Faradaic processes in the region between 0.05 V and 0.4 V RHE for Pt(111) electrodes in acidic media using the common measurement schemes. Only in some cases it has been possible to do that, *e.g.*, using very high frequencies and special equipment.⁶⁹

However, our impedance analysis (see the ESI,† Section S2, for further information about the equivalent electric circuit) shows that in the case of Pt(331) it is possible to distinguish several Faradaic adsorption processes with different time constants. Fig. 2A shows a schematic representation of a physical model (equivalent electric circuit), known for the reversible surface limited adsorption, used in this work (see ref. 70 and the ESI† for the detailed discussion of this model). It comprises three branches. The first branch consists of the impedance of the so-called constant phase element (CPE), $Z_{\text{dl}} = 1/C_{\text{dl}}'(j\omega)^{-\phi}$, where C_{dl}' is proportional to the double layer capacitance (C_{dl}), and ϕ is the exponent accounting for the frequency dispersion of the double layer (see detailed information related to this parameter in ref. 56). The other two branches consist of the series combination of the resistances of adsorption, R_i , and capacitances of adsorption, C_i . They account for slower adsorption processes with different time constants. An additional resistance was necessary in parallel to the double layer impedance to account for the oxygen reduction reaction in the oxygen saturated electrolytes, similar to the situation described in ref. 56, 71 and 72 (not shown in Fig. 2A). R_s stands for the uncompensated resistance.

It turned out that the model presented in Fig. 2A fits well with all the potentiodynamic impedance spectra obtained in this work. Fig. 2B and C show the typical examples of the impedance spectra of Pt(331) electrodes obtained in Ar-saturated and O₂-saturated 0.1 M HClO₄ electrolytes together with the fitting results.

Fig. 3 presents the dependencies of the parameters of the equivalent circuit (shown in Fig. 2A) on the electrode potential, which are of primary importance to elucidate the nature of adsorbates at the electrode surface. Those parameters are the capacitances of adsorption, designated as C_1 (Fig. 3A) and C_2 (Fig. 3B), as well as $C_{\text{dl}}' \approx C_{\text{dl}}$ (Fig. 3C), which can be approximated as the double layer capacitance, as ϕ is relatively close to 1. While it is possible to extract additional information from $\varphi(E)$ dependencies,⁵⁶ we simplify the analysis to maintain the main focus of this work. The adsorption resistances are not considered, as they largely correlate with the respective capacitances and do not provide further necessary information for the current study. Therefore, only the adsorption capacitances will be used for further analysis.



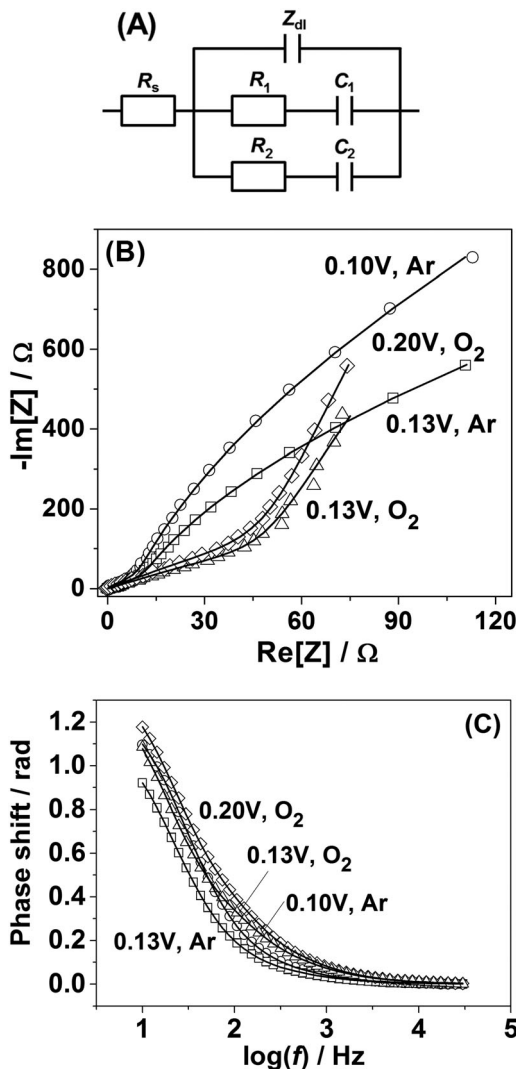


Fig. 2 (A) Equivalent electric circuit schematically describing the adsorption processes at the interface between Pt(331) electrodes and all types of electrolytes used in this work. In the case of O_2 -saturated electrolytes an additional charge transfer resistance is applied to account for the ORR. See the designation of all the elements in the main text. (B and C) Examples of the impedance spectra of Pt(331) in contact with Ar-saturated and O_2 -saturated 0.1 M HClO_4 electrolytes (open symbols) together with the fitting results (lines). The spectra are corrected for the uncompensated resistance R_s .

As can be seen in Fig. 3A, the adsorption capacitance C_1 demonstrates a well-pronounced peak at $\sim 0.13 \text{ V}$ with the value of ca $1500 \mu\text{F cm}^{-2}$. Integration of the $C_1(E)$ dependence between 0.07 V and 0.4 V gives the charge of ca. $60 \mu\text{C cm}^{-2}$.

Fig. 3B shows the dependence of another adsorption capacitance, $C_2(E)$, as a function of electrode potential. While the shape and the maximal values of this curve are drastically different when compared with $C_1(E)$, the peak position is exactly the same: $\sim 0.13 \text{ V}$. Integration of the $C_2(E)$ between 0.07 V and 0.4 V gives a charge of $\sim 30 \mu\text{C cm}^{-2}$, as shown in the figure.

Finally, the “approximate” double layer capacitance demonstrates unusually high values in the potential region between 0.07 V and 0.4 V with the peak at $\sim 0.13 \text{ V}$ (Fig. 4C). The high

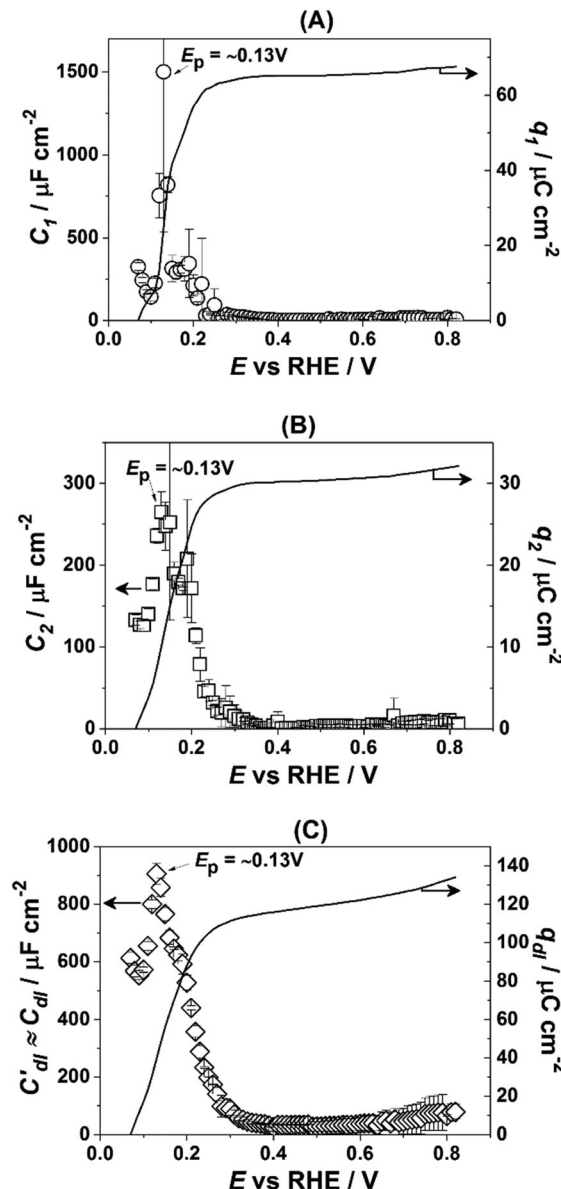


Fig. 3 Dependencies of the parameters of the equivalent electric circuit shown in Fig. 2A. They reflect different adsorption processes at the Pt(331) surface in contact with 0.1 M HClO_4 . (A and B) Adsorption capacitances C_1 and C_2 . (C) The “approximate” double layer capacitance which includes an unseparable contribution from the very fast underpotential deposition/desorption of hydrogen atoms. Solid lines represent the integrated charges obtained from the capacitance values.

values of this parameter are due to the fact that it is not possible to separate fast H-adsorption/desorption from the double layer response completely. Formal integration of this curve in this potential range gives values which are slightly above $\sim 110 \mu\text{C cm}^{-2}$. Thus the sum of the charges obtained from PDEIS measurements ($60 + 30 + 110 = 200 \mu\text{C cm}^{-2}$) is very close to the voltammetric charge obtained from the CV in this range ($\sim 190 \mu\text{C cm}^{-2}$). The slight differences are due to the fact that the CV data were corrected for the background.

However, in the above-presented data there are no direct indications of the adsorption processes with the adsorption

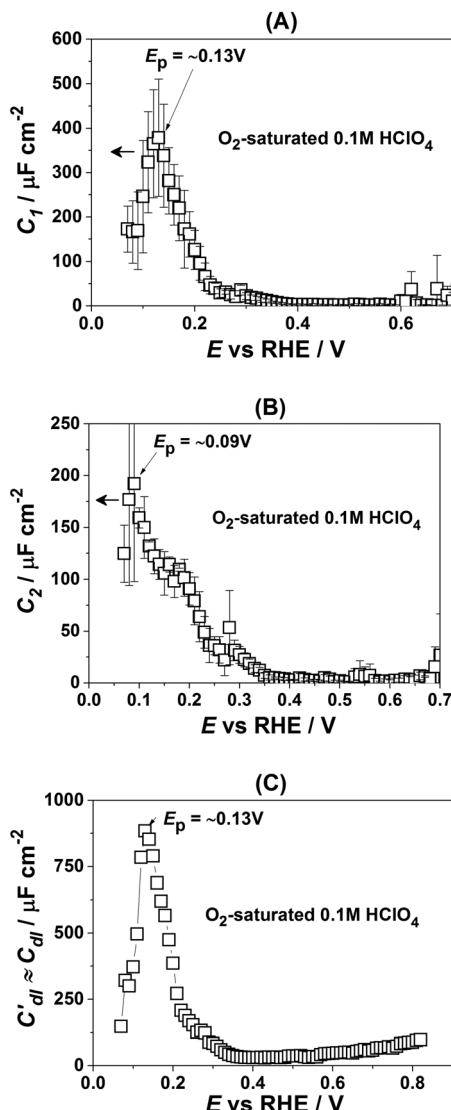


Fig. 4 Characterization of adsorption phenomena at Pt(331) electrodes in O_2 -saturated $HClO_4$ electrolytes. (A and B) Adsorption capacitances C_1 and C_2 . (C) The “approximate” double layer capacitance which includes an unseparable contribution from the very fast underpotential deposition/desorption of hydrogen atoms. Solid lines represent the integrated charges obtained from the capacitance values.

capacitances C_1 and C_2 . It is well accepted that ClO_4^- anions cannot be specifically adsorbed in this system. Therefore, both C_1 and C_2 can represent slower adsorption of hydrogen, or alternatively they can reveal the adsorption of $*OH$ at two different types of sites. Finally, one of these capacitances can reveal $*OH$ -adsorption while the other represents the slower adsorption of hydrogen. In order to assign the adsorption capacitances to the specific processes we use the previously documented fact^{56,71,72} that OH-adsorption on Pt is very sensitive to the presence of the dissolved O_2 as $*OH$ is also an intermediate in the ORR. In the presence of oxygen the OH-adsorption isotherms are shifted to more negative potentials.

Fig. 4 shows how the capacitance peaks change in O_2 -saturated 0.1 M $HClO_4$. As can be seen from Fig. 4, in the presence of

dissolved oxygen the dependencies of the observed parameters are different. While all three curves look slightly “depressed”, the positions of the main peaks in Fig. 4A and C remain the same. However, the position of the main peak in Fig. 4B is shifted by ~ 40 mV towards more negative potentials. Thus, this peak in the $C_2(E)$ curve is highly sensitive to the presence of the molecular oxygen in the electrolyte.

Discussion

As mentioned above, the working hypothesis of this study is that at stepped Pt surfaces, particularly Pt(331), the steps are blocked by “oxygenated” species at the PEMFC critical potential of 0.9 V (RHE) influencing the electronic structure and the performance of the catalytic sites at the (111) facets. The data presented in the previous section in general confirm this hypothesis. It should be noted that the adsorption of oxygenated species, *e.g.* $*OH$, likely starts at the potentials close to 0.1 V (RHE). The first evidence of this is provided by cyclic voltammetry data. Formally, Pt(331) has approximately the same amount of adsorption sites as Pt(111). The only difference is that steps change the coordination number of some of the surface atoms leading to a non-uniform adsorption energy distribution along the surface. However, while it is well known that the maximal charge associated with adsorption/desorption of hydrogen atoms for Pt(111) terraces is $\sim 160 \mu C \text{ cm}^{-2}$, the integrated charge in that potential region for Pt(331) is $\sim 30 \mu C \text{ cm}^{-2}$ higher, both in perchloric and sulfuric acids. Assuming that the specific adsorption of perchlorate anions is unlikely on Pt-surfaces,⁵⁶ this excessive charge can be associated with the specific adsorption/desorption of $*OH$ from water.

PDEIS data support the idea that the excessive charge of $\sim 30 \mu C \text{ cm}^{-2}$ is due to adsorption of $*OH$ in the potential range between 0.07 V and 0.4 V. In 0.1 M $HClO_4$ using impedance analysis it was possible to distinguish at least two adsorption processes other than fast H-adsorption, which is indistinguishable from the double layer response (Fig. 3). Surprisingly, the integration of one of the associated capacitance dependencies (Fig. 3B), namely $C_2(E)$, gives approximately the same charge, $\sim 30 \mu C \text{ cm}^{-2}$, which is observed as the additional one in the CV data. Furthermore, under the ORR conditions the peak in $C_2(E)$ is shifted towards more negative potentials (Fig. 4B). This behavior is typical in the case of adsorbed $*OH$ as reported earlier,^{56,71,72} as $*OH$ is also an ORR intermediate. Notably, the positions of the other peaks, which can therefore be associated with H-adsorption/desorption, are not affected by the molecular oxygen as it is not directly involved in these processes (Fig. 3A and C).

Thus, high values of $C_{dl}(E)$ are associated with a very fast adsorption of hydrogen, C_1 represents a slower adsorption of hydrogen at different types of sites and C_2 accounts for the OH-adsorption.

Based on the obtained data, it is now important to elucidate possible adsorbate structures, involving $*H$, $*OH$ and also $*O$, explaining the main impedance and voltammetric features in



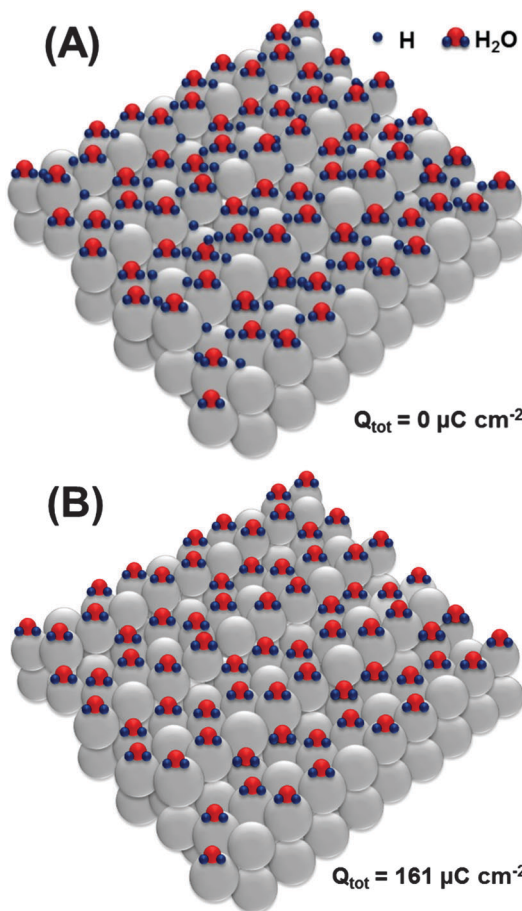


Fig. 5 Proposed adsorbate structures at the Pt(331) electrode surface developed during the oxidation sweep in the potential region between 0.05 V and 0.4 V (RHE), without involving a possible concurrent $^*\text{OH}$ adsorption. Oxidation of the adsorbed hydrogen requires only $\sim 161 \mu\text{C cm}^{-2}$.

all potential regions used in this work. We start with the most probable structure at the surface of Pt(111) (Fig. 5A). The existence of ordered superstructures consisting of surface water and adsorbed $^*\text{H}$ species is supported by DFT calculations;⁷³ however, we use it for Pt(331) as the first approximation, as it can be affected by different coordinations at steps on the Pt[3(111) \times (111)] surface.

Oxidation of the adsorbed hydrogen corresponds to the charge of $\sim 161 \mu\text{C cm}^{-2}$, as shown in Fig. 5B.

Adsorption sites on the steps of Pt(331) are the “weakest links” towards oxidation, which is equivalent in this system to the adsorption of oxygenated species. Interestingly, oxidation of H_2O molecules at steps of every third atom (Fig. 6) is equivalent to the total anodic charge equal to $\sim 187 \mu\text{C cm}^{-2}$, *i.e.* very close to the charge measured by CV within the relevant potential region ($\sim 190 \mu\text{C cm}^{-2}$). Accordingly, we hypothesize that structures close to those shown in Fig. 6 exist at the potential of ca 0.4 V (RHE).

Further oxidation would involve the second row of platinum atoms on the Pt(111) facets. Again, we hypothesize that oxidation starts at every third platinum atom as schematically shown in Fig. 7A, leading to the formation of an OH-layer with

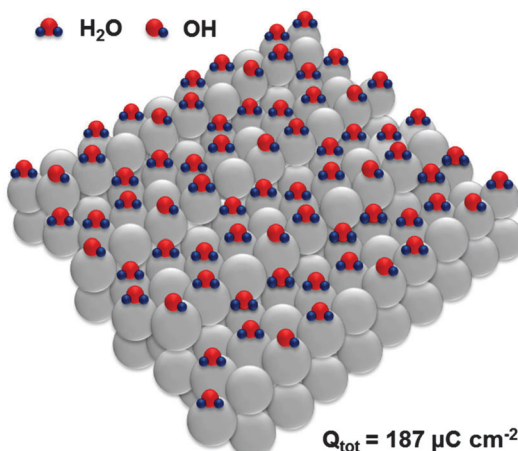


Fig. 6 Proposed adsorbate structures at the Pt(331) electrode surface developed during the oxidation sweep in the potential region between 0.05 V and 0.4 V (RHE), involving a possible concurrent $^*\text{OH}$ adsorption. Oxidation of the adsorbed hydrogen together with OH-adsorption should give the anodic charge of $\sim 187 \mu\text{C cm}^{-2}$.

simultaneous oxidation of $^*\text{OH}$ at steps to $^*\text{O}$. The formation of the structure shown in Fig. 7A corresponds to the total anodic charge of $\sim 241 \mu\text{C cm}^{-2}$. Interestingly, this charge was obtained by integration of the CV shown in Fig. 1 at the potential of ca 0.8 V (RHE), where the onset of a new oxidation wave can be seen.

Finally, at the potential of ~ 0.9 V, the integrated anodic charge from the voltammograms is $\sim 280 \mu\text{C cm}^{-2}$. This might correspond to the structure shown in Fig. 7B, with a slightly increased coverage of $^*\text{O}$ and $^*\text{OH}$ at the steps and terraces, respectively.

While the proposed structures presented in Fig. 5–7 are largely hypothetical, as there are unfortunately no straightforward means to directly visualize the real adsorbate structures *in situ*, they can explain CV and PDEIS data with a high accuracy. Nevertheless, the main results of the combined CV and PDEIS studies are that $^*\text{OH}$ adsorption at Pt(331) starts as early as 0.1 V (RHE) and that at the potential of 0.9 V, critical for PEMFC applications, all the steps are indeed blocked by $^*\text{O}$. This provides further evidence that the active sites for the ORR are located at (111) terraces,^{20,55} which confirms earlier hypotheses and previous theoretical studies showing that the (111) terraces are responsible for the high activity of many extended Pt surfaces and some “normal shape” convex nanoparticles. This provides a direct input to the theoretical modelling, which can involve quantum chemistry calculations, as well as to future combined theoretical and experimental studies: adsorbed $^*\text{O}$ at the surface of non-uniform ORR electrocatalysts with a significant number of under-coordinated sites should be taken into account. Our experiment with the Pt(331) surface, where only a few types of “on-top” sites exist, shows that immobile $^*\text{O}$ at steps likely and largely contributes to the high activity of Pt(331), as each atomic row meets the atomic row with the adsorbed $^*\text{O}$ at (111) terraces (where the active sites should be located). This is the main difference

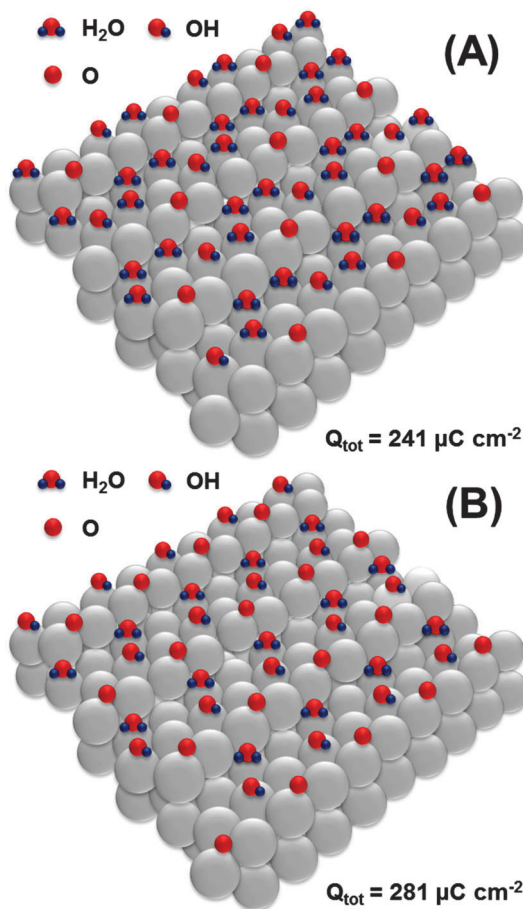


Fig. 7 Proposed adsorbate structures at the Pt(331) electrode surface developed at the potentials between 0.8 V and 0.9 V (RHE).

between the status of Pt(111) and Pt(331) surfaces at the benchmark potentials close to 0.9 V RHE.

Conclusions

Combined CV and PDEIS studies confirm that OH-adsorption on the most active Pt ORR electrocatalysts in acidic media, Pt(331), starts as early as at *ca.* 0.1 V (RHE). At the key electrode potential of 0.9 V (RHE) for PEMFC applications, almost all the step sites are blocked by the adsorbed *O. This fact supports the hypothesis that the most active sites for the ORR should be located at the (111) terraces. Moreover, *O should largely contribute to the high activity of the (111) terraces. Further investigations, for instance, explicit calculations using density functional theory, are necessary to identify the exact locations and properties of the resulting catalytic sites at these terraces.

Notes and references

- 1 M. Winter and R. J. Brodd, *Chem. Rev.*, 2004, **104**, 4245.
- 2 *Fuel Cell Catalysis: A Surface Science Approach*, ed. M. Koper, John Wiley & Sons, Inc., Hoboken, 2008.
- 3 X. Yu and S. Ye, *J. Power Sources*, 2007, **172**, 145.
- 4 I. E. L. Stephens, A. S. Bondarenko, U. Grønbjerg, J. Rossmeisl and I. Chorkendorff, *Energy Environ. Sci.*, 2012, **5**, 6744.
- 5 Y. Nie, L. Li and Z. Wei, *Chem. Soc. Rev.*, 2015, **44**, 2168.
- 6 A. Rabis, P. Rodriguez and T. J. Schmidt, *ACS Catal.*, 2012, **2**, 864.
- 7 A. Hitotsuyanagi, M. Nakamura and N. Hoshi, *Electrochim. Acta*, 2012, **82**, 512.
- 8 H. A. Gasteiger, S. S. Kocha, B. Sompalli and F. T. Wagner, *Appl. Catal., B*, 2005, **56**, 9.
- 9 V. R. Stamenkovic, B. Fowler, B. S. Mun, G. Wang, P. N. Ross, C. A. Lucas and N. M. Markovic, *Science*, 2007, **315**, 493.
- 10 F. Calle-Vallejo, M. T. M. Koper and A. S. Bandarenka, *Chem. Soc. Rev.*, 2013, **42**, 5210.
- 11 *A Handbook of Fuel Cells, Fundamentals Technology and Applications*, ed. W. Vielstich, A. Lamm and H. Gasteiger, Wiley, West Sussex, 2003.
- 12 *Catalysis in Electrochemistry: From Fundamental Aspects to Strategies for Fuel Cell Development*, ed. E. Santos and W. Schmickler, John Wiley & Sons, New Jersey, 2015.
- 13 A. M. Gómez-Marín and J. M. Feliu, *Catal. Today*, 2015, **244**, 172.
- 14 A. U. Nilekar and M. Mavrikakis, *Surf. Sci.*, 2008, **602**, L89.
- 15 Y. Wang, K. S. Chen, J. Mishler, S. C. Cho and X. C. Adroher, *Appl. Energy*, 2011, **88**, 981.
- 16 M. Watanabe, D. A. Tryk, M. Watsisaka and H. Yanom H. Uchida, *Electrochim. Acta*, 2012, **84**, 187.
- 17 H. A. Gasteiger and N. M. Markovic, *Science*, 2009, **324**, 48.
- 18 M. K. Debe, *Nature*, 2012, **486**, 43.
- 19 M. H. Shao, K. Shoemaker, A. Peles, K. Kaneko and L. Protsailo, *J. Am. Chem. Soc.*, 2010, **132**, 9253.
- 20 A. S. Bandarenka, H. A. Hansen, J. Rossmeisl and I. E. L. Stephens, *Phys. Chem. Chem. Phys.*, 2014, **16**, 13625.
- 21 *PEM Fuel Cell Electrocatalysts and Catalyst Layers*, ed. J. Zhang, Springer London, London, 2008.
- 22 N. M. Markovic and P. N. Ross, *Electrochim. Acta*, 2000, **45**, 4101.
- 23 Z. Duan and G. Wang, *Phys. Chem. Chem. Phys.*, 2011, **13**, 20178.
- 24 J. Larminie and A. L. Dicks, *Fuel Cell Systems Explained*, John Wiley and Sons Inc., Hoboken, NJ, 2nd edn, 2003.
- 25 A. S. Bandarenka and M. T. M. Koper, *J. Catal.*, 2013, **308**, 11.
- 26 J. Greeley and J. K. Nørskov, *J. Phys. Chem. C*, 2009, **113**, 4932.
- 27 J. B. Henry, A. Maljusch, M. Huang, W. Schuhmann and A. S. Bondarenko, *ACS Catal.*, 2012, **2**, 1457.
- 28 D. Li, C. Wang, D. S. Strmenik, D. V. Tripkovic, X. Sun, Y. Kang, M. Chi, J. D. Snyder, D. van der Vliet, Y. Tsai, V. R. Stamenkovic, S. Sun and N. M. Markovic, *Energy Environ. Sci.*, 2014, **7**, 4061.
- 29 A. J. Appleby, *Catal. Rev.*, 1970, **4**, 221.
- 30 K. Kinoshita, *Electrochemical Oxygen Technology*, Wiley, New York, 1992.
- 31 Y. Dai and S. Chen, *ACS Appl. Mater. Interfaces*, 2015, **7**, 823.



32 V. R. Stamenkovic, B. Simon Mun, K. J. J. Mayrhofer, P. N. Ross and N. M. Markovic, *J. Am. Chem. Soc.*, 2006, **128**, 8813.

33 O. T. Holton and J. W. Stevenson, *Platinum Met. Rev.*, 2013, **57**, 259.

34 J. K. Nørskov, J. Rossmeisl, A. Logadottir, L. Lindqvist, J. R. Kitchin, T. Bligaard and H. Jónsson, *J. Phys. Chem. B*, 2004, **108**, 17886.

35 *Fuel Cell Technology Handbook*, ed. G. Hoogersy, CRC Press, Boca Raton, 2002.

36 J. Greeley, I. E. L. Stephens, A. S. Bondarenko, T. P. Johansson, H. A. Hansen, T. F. Jaramillo, J. Rossmeisl, I. Chorkendorff and J. K. Nørskov, *Nat. Chem.*, 2009, **1**, 552.

37 L. M. C. Pinto, P. Quaino, M. D. Arce, E. Santos and W. Schmickler, *ChemPhysChem*, 2014, **15**, 2003.

38 G. S. Karlberg, *Phys. Rev. B*, 2006, **74**, 153414.

39 A. Michaelides and P. Hu, *J. Am. Chem. Soc.*, 2001, **123**, 4235.

40 A. Michaelides and P. Hu, *J. Chem. Phys.*, 2001, **114**, 513.

41 F. Calle-Vallejo, J. Tymoczko, V. Colic, Q. H. Vu, M. D. Pohl, K. Morgenstern, D. Loffreda, P. Sautet, W. Schuhmann and A. S. Bandarenka, *Science*, 2015, **350**, 185.

42 P. Strasser, S. Koh, T. Anniyev, J. Greeley, K. More, C. Yu, Z. Liu, S. Kaya, D. Nordlund, H. Ogasawara, M. F. Toney and A. Nilsson, *Nat. Chem.*, 2010, **2**, 454.

43 V. Stamenkovic, B. S. Mun, K. J. J. Mayrhofer, P. N. Ross, N. M. Markovic, J. Rossmeisl, J. Greeley and J. K. Nørskov, *Angew. Chem., Int. Ed.*, 2006, **45**, 2897.

44 M. Escudero-Escribano, A. Verdaguer-Casadevall, P. Malacrida, U. Grønbjerg, B. P. Knudsen, A. K. Jepsen, J. Rossmeisl, I. E. L. Stephens and I. Chorkendorff, *J. Am. Chem. Soc.*, 2012, **134**, 16476.

45 C. Zhang, S. Y. Hwang and Z. Peng, *J. Mater. Chem. A*, 2014, **2**, 19778.

46 Y. Takesue, M. Nakamura and N. Hoshi, *Phys. Chem. Chem. Phys.*, 2014, **16**, 13774.

47 T. Rurigaki, A. Hitotsuyanagi, M. Nakamura, N. Sakai and N. Hoshi, *J. Electroanal. Chem.*, 2014, **716**, 58.

48 A. Kuzume, E. Herrero and J. M. Feliu, *J. Electroanal. Chem.*, 2007, **599**, 333.

49 N. P. Lebedeva, A. Rodes, J. M. Feliu, M. T. M. Koper and R. A. van Santen, *J. Phys. Chem. B*, 2002, **106**, 9863.

50 N. P. Lebedeva, M. T. M. Koper, J. M. Feliu and R. A. van Santen, *J. Phys. Chem. B*, 2002, **106**, 12938.

51 J. L. Gland and V. N. Korchak, *Surf. Sci.*, 1978, **75**, 733.

52 G. García and M. T. M. Koper, *J. Am. Chem. Soc.*, 2009, **131**, 5384.

53 J. Yue, Z. Du and M. Shao, *J. Phys. Chem. Lett.*, 2015, **6**, 3346.

54 M. J. T. C. van der Niet, N. Garcia-Araez, J. Hernández, J. M. Feliu and M. T. M. Koper, *Catal. Today*, 2013, **202**, 105.

55 J. Greeley, J. Rossmeisl, A. Hellman and J. K. Nørskov, *Z. Phys. Chem.*, 2007, **221**, 1209.

56 A. S. Bondarenko, I. E. L. Stephens, H. A. Hansen, F. J. Perez-Alonso, V. Tripkovic, T. P. Johansson, J. Rossmeisl, J. K. Nørskov and I. Chorkendorff, *Langmuir*, 2011, **27**, 2058.

57 G. A. Kimmel, N. G. Petrik, Z. Dohnalek and B. D. Kay, *Phys. Rev. Lett.*, 2005, **95**, 166102.

58 K. J. P. Schouten, M. J. T. C. van der Niet and M. T. M. Koper, *Phys. Chem. Chem. Phys.*, 2010, **12**, 15217.

59 E. Codorniu-Hernandez and P. G. Kusalik, *J. Am. Chem. Soc.*, 2012, **134**, 532.

60 A. Picolin, C. Busse, A. Redinger, M. Morgenstern and T. Michely, *J. Phys. Chem. C*, 2009, **113**, 691.

61 N. M. Markovic and P. N. Ross, *Surf. Sci. Rep.*, 2002, **45**, 117.

62 A. S. Bondarenko, *Anal. Chim. Acta*, 2012, **743**, 41.

63 B. A. Boukamp, *J. Electrochem. Soc.*, 1995, **142**, 1885.

64 C. A. Schiller, F. Richter, E. Gültzow and N. Wagner, *Phys. Chem. Chem. Phys.*, 2001, **3**, 374.

65 B. B. Berkes, A. Maljusch, W. Schuhmann and A. S. Bondarenko, *J. Phys. Chem. C*, 2011, **115**, 9122.

66 B. B. Berkes, J. B. Henry, M. Huang and A. S. Bondarenko, *ChemPhysChem*, 2012, **13**, 3210.

67 V. Climent, N. M. Markovic and P. N. Ross, *J. Phys. Chem. B*, 2000, **104**, 3116.

68 G. A. Ragoisha and A. S. Bondarenko, *Electrochim. Acta*, 2005, **50**, 1553.

69 E. Sibert, R. Faure and R. Durand, *Electrochim. Commun.*, 2001, **3**, 181.

70 B. B. Berkes, G. Inzelt, W. Schuhmann and A. S. Bondarenko, *J. Phys. Chem. C*, 2012, **116**, 10995.

71 A. S. Bondarenko, I. E. L. Stephens, L. Bech and I. Chorkendorff, *Electrochim. Acta*, 2012, **82**, 517.

72 J. Tymoczko, V. Colic, A. S. Bandarenka and W. Schuhmann, *Surf. Sci.*, 2015, **631**, 81.

73 E. Skulason, V. Tripkovic, M. E. Björketun, S. Gudmundsdottir, G. Karlberg, J. Rossmeisl, T. Bligaard, H. Jonsson and J. K. Nørskov, *J. Phys. Chem. C*, 2010, **114**, 18182.

